RESEARCH ARTICLE

Emulative, coherent, and causal dynamics between large-scale brain networks are neurobiomarkers of Accelerated Cognitive Ageing in epilepsy

Antoine Bernas[1,2]*, Lisanne E. M. Breuer[3], Albert P. Aldenkamp[1,2,3], Svitlana Zinger[1]

1 Department of Electrical Engineering, Eindhoven University of Technology, Eindhoven, The Netherlands, **2** Department of Cognitive Neuropsychiatry and Clinical Neurosciences, School for Mental Health and Neuroscience, Maastricht University, Maastricht, The Netherlands, **3** Department of Research and Development, Epilepsy Centre Kempenhaeghe, Heeze, The Netherlands

* antoine.bernas1@gmail.com

Abstract

Accelerated cognitive ageing (ACA) is an ageing co-morbidity in epilepsy that is diagnosed through the observation of an evident IQ decline of more than 1 standard deviation (15 points) around the age of 50 years old. To understand the mechanism of action of this pathology, we assessed brain dynamics with the use of resting-state fMRI data. In this paper, we present novel and promising methods to extract brain dynamics between large-scale resting-state networks: the emulative power, wavelet coherence, and granger causality between the networks were extracted in two resting-state sessions of 24 participants (10 ACA, 14 controls). We also calculated the widely used static functional connectivity to compare the methods. To find the best biomarkers of ACA, and have a better understanding of this epilepsy co-morbidity we compared the aforementioned between-network neurodynamics using classifiers and known machine learning algorithms; and assessed their performance. Results show that features based on the evolutionary game theory on networks approach, the emulative powers, are the best descriptors of the co-morbidity, using dynamics associated with the default mode and dorsal attention networks. With these dynamic markers, linear discriminant analysis could identify ACA patients at 82.9% accuracy. Using wavelet coherence features with decision-tree algorithm, and static functional connectivity features with support vector machine, ACA could be identified at 77.1% and 77.9% accuracy respectively. Granger causality fell short of being a relevant biomarker with best classifiers having an average accuracy of 67.9%. Combining the features based on the game theory, wavelet coherence, Granger-causality, and static functional connectivity- approaches increased the classification performance up to 90.0% average accuracy using support vector machine with a peak accuracy of 95.8%. The dynamics of the networks that lead to the best classifier performances are known to be challenged in elderly. Since our groups were age-matched, the results are in line with the idea of ACA patients having an accelerated cognitive decline. This classification pipeline is promising and could help to diagnose other neuropsychiatric disorders, and contribute to the field of psychoradiology.

1 Introduction

Cognitive impairment is a common comorbidity in epilepsy. It is estimated that 65% of all patients show impairment in cognition, accounting for about half of the burden of disease [1]. Using fMRI, research has mainly focused on specific cognitive impairments, and correlated them with aberrant functional connectivity in brain areas involved in focal epilepsy. For instance, in rolandic epilepsy, language and motor-related functions are impaired, and were linked to a reduced functional connectivity between sensorimotor network and Broca's area [2]. Also already at young age, children with frontal lobe epilepsy complicated by cognitive impairment (memory) showed decrease in frontal lobe connectivity [3]. In an elderly population, the decline in cognitive abilities is also clearly present, yet often neglected [4]. This more general cognitive decline is often due to long-term accumulating effects, i.e. early onset and chronic epilepsy, and heavy use of anti-epileptic drugs, which hinders healthy mental ageing [5]. This is often described as a chronic/accumulative model of cognitive decline, and viewed as a form of dementia [6]. More recently, another model of cognitive decline in elderly has been presented. It is different from the chronic decline since it relates to epilepsy that has a late onset, where the decline is more abrupt and occurs soon after the diagnosis of epilepsy. Also, it does not seem to degrade the crystalized cognitive functions such as long-term memory and language abilities; but rather the fluid intelligence: perceptual reasoning and processing speed. This fast mental ageing is coined 'accelerated cognitive ageing', or ACA [7, 8]. Even though the clinical characteristics of the ACA comorbidity has been described, the brain mechanism of action of the pathology remains unclear. This is why in this study we assess, using fMRI, different dynamic parameters of large-scale networks that could help describing neuronal mechanisms behind the decline.

The brain has been proven to efficiently work in functionally connected networks, i.e. the aggregation of multiple region of interests (ROIs) [9, 10]. Also, the links between brain activity and behavior/cognition are often better analyzed through the use of large-scale networks [11–14]. Therefore, the resting-state network (RSN) dynamics are informative features in neuropsychiatric disorders and can be used as neurobiomarkers. Between-network neurodynamics analysis can be performed using network time series from a spatial independent component analysis (ICA), a reliable data-driven method [15, 16]. In a seed-based approach (voxel-to-voxel, or ROI-to-ROI), the seeds or ROIs have to be defined a priori, and this can be quite inter-subject variable, especially for resting-state (task-free) fMRI. Hence the choice of ICA decomposition for extracting the functional brain RSNs and their activity time courses is favorable for robust rs-fMRI group analysis, and is preferred here.

After extracting the time series per network, diverse methods can be applied to estimate the dynamics of these networks. Currently, to find the abnormalities in brain functioning of patients with neuropsychiatric disorders, research has mainly focused on static functional connectivity (sFC), i.e. pairwise correlations between the functional networks' activity. It has been shown that at rest the default-mode network is involved in the impairment in autism [17, 18]; and the attention and executive networks in attention deficit hyperactivity disorder (ADHD) [19, 20]. But for more complex mental illnesses (e.g. depression or schizophrenia) dynamic measures of the brain connectivity seem to be more robust biomarkers [21, 22].

In that regard, effective connectivity (EC) can be used [23, 24]. The EC, or measure of causality in brain connectivity, has already shown promising results for autism and depression [25, 26]. However, in terms of cognitive decline in the ageing process, clear causal dynamics indicators are missing. Liu et al. have shown links between cognitive decline and changes in Granger causality (a measure of EC) of cognitive networks in mild cognitive impairment [27]. Using a different—more hypothesis driven—causal measurement, the dynamic causal

modeling (DCM), Tsvetanov et al. showed that differences in between and within large-scale resting-state networks were linked to cognitive performance in elderly [28]. More precisely they demonstrated that the DCM of the default mode, dorsal attention and salience networks (DMN, DAN, SN) where associates with increased influence on cognitive functioning—that tends to decline—in healthy elderly. Another study showed the involvement of DMN and SN in the cognitive decline in cognitively impaired elderly using also the DCM approach [29].

More recently, to assess neuro- and psycho-pathology, the dynamic functional connectivity (dFC) methods have been used as well [21, 30–34]. These are similar to the sFC but when correlation coefficients are calculated over different time windows. By sliding these windows throughout the full time series, one can extract the dFC between the networks being assessed [35, 36]. This method of analysis has been for example applied to extract abnormal brain states in the study of schizophrenia, which has stronger classification power as compared to classic static functional connectivity [37]. The same methods can also be applied in the frequency domain, and the sliding windows approach can be applied on Fourier spectra, giving rise to spectrograms. And similar spectro-temporal analysis of wavelet coherence has not been much used in fMRI studies. Chang and Glover have shown added value in assessing non-stationarity and time-varying anti-correlation between DMN and cognitive networks, using wavelet coherence [38]. To relate to cognitive decline, only one study used wavelet coherence analysis of near-infrared spectroscopic signals to infer changes in brain functional connectivity in respect to performance in vigilance task, suggesting that decreased attention—a known phenomenon in ageing, and probably associated to cognitive decline—was attributed to reduced phase coherence between left prefrontal region and sensorimotor area. In a previous rs-fMRI study, we have successfully shown that coherent patterns, using wavelet coherence, are also impaired in autism; and the duration of these coherent patterns can be used as biomarker of the disorder [39].

Finally, evaluation of brain dynamics can be done through an evolutionary game theory approach on brain networks (EGN). Madeo and his colleagues were first to implement the methods on BOLD fMRI signals [40]. They demonstrated that EGN model is able to mimic functional connectivity dynamics, which could then be used to simulate the impact of brain network lesions onto the networks' dynamics. This was done using simulated time series and real fMRI data from healthy subjects. Here, we present the first fMRI study where the EGN model is applied to a clinical population in order to see if network emulative powers (parameters of the model) can be descriptors of ACA.

The goal of our research is to define the most informative fMRI neurobiomarkers for ACA based on neurodynamics metrics. To achieve this, we use these metrics as features and train classifiers for ACA detection. The features that lead to the best classification results can then be considered the best descriptors of ACA. Therefore, in our study, the aforementioned neurodynamics techniques are used to extract fMRI-base dynamic features of brain networks, which are then fed to classifiers, to train and validate them. Decision tree, linear discriminant analysis, the K-nearest neighbors and the support vector machine are common supervised machine learning algorithms that divide the training data in two or more categories. Counting the number of correct binary classifications, in the validation dataset, leads to a certain amount of accuracy, i.e. the percentage of participants that has been correctly assigned to their respective label (in our case, ACA or non-ACA/controls); which shows the descriptive power of the features, and to a certain extent its usability in a clinical environment. Convolutional neural network (CNN) can also be used to extract and test specific brain features using resting-state fMRI. It has already been tested in order to help diagnosing neuropsychiatric disorders, such as autism [41], ADHD [42], and schizophrenia [43]. An important drawback of this classification technique is that it usually needs a large amount of data to be trained upon; Moreover, the

understanding and explanation of the feature maps obtained at different CNN layers can be arduous and troublesome. This is why we used here the aforementioned supervised machine learning algorithms and assessed the performance of classifiers using neurodynamics metrics, in order to find the best biomarkers of the ACA comorbidity, which if replicated could help describing the mechanism of action of the cognitive decline. Testing the classification pipeline we describe here, in a bigger dataset stratified, e.g. through duration since onset of epilepsyor age ranges, could even help predict the course of the decline and its severity.

2 Materials and methods

Fig 1 provides an overview of the Materials and methods section, and short descriptions of the steps of the study pipeline. The study was approved by the Dutch Medical Research Ethical Committee (MREC) of Maxima Medical Center. All subjects signed informed consent and gave permission to use the clinical data for scientific purposes.

2.1 Dataset, preprocessing, and brain network extraction

The dataset contains two resting-state, RS1 and RS2, sessions acquired from 10 ACA patients and 14 controls. Prior to RS2, a silent word generation task was performed for 7 min. Dynamics features that show significant differences between the two populations in RS1 as well as in RS2, would show robustness of the features as biomarkers. Indeed, since the task in-between resting-states was cognitively demanding, such features would have discriminant power regardless of the brain fatigue the participants experienced. On the contrary, the difference in findings between RS1 and RS2 could shed light on the cognitive reserve capacity of the ACA patients, which can be of interest too. Table 1 shows the demographics of the participants, the type of epilepsy, and the deterioration scores, i.e. cognitive decline, for Full-Scale IQ, Perceptual Reasoning Index, and Verbal Comprehension Index (respectively FSIQ, PRI, and VCI). Deterioration scores were calculated by subtracting the estimated premorbid IQ scores from the actual scores, i.e. WAIS-IV (actual) IQ-scores—OPIE-IV (premorbid) IQ-scores [44, 45].

The T1-weighted anatomical images were acquired using a 3.0 T imaging system (Philips Achieva) with a 3D Fast Field Echo (FFE) sequence: echotime (TE) = 3.8 ms, repetition time (TR) = 8.3 ms; Inversion time (TI) = 1035 ms; field of view (FOV) = 240x240 mm^2, with 180 sagittal slices; flip-angle (FA) = 8 deg.; and voxel size = 1x1x1 mm^3; with SENSE factor of 1.5, and scan duration of 6:02 min. Functional MRI-data were acquired using multi-echo echo-planar imaging (ME-EPI) sequences with 3 echoes: TEs = 12, 35, 58 ms, TR = 2 s; FA = 90 deg.; SENSE factor = 2.7; 208 dynamics for a total of 7 minutes; 27 axial slices (with no gap), 64x64 matrix FOV, with a 3.5x3.5x4.5 mm^3 voxel size. The raw multi-echo fMRI data were first
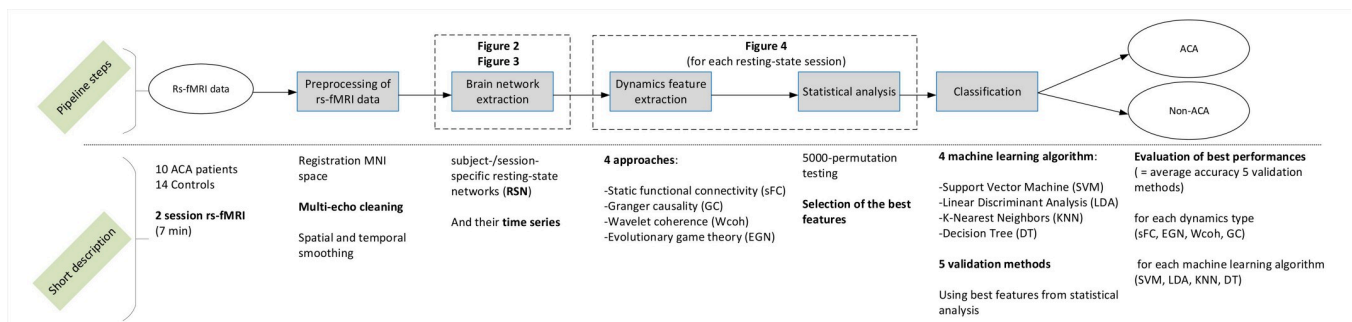

Fig 1. Overview of the methodology.

Table 1. Demographic and clinical information of the participants.

	ACA	Healthy controls
Age in years M (SD) range	61.3 (8.9)	62.2 (9.8)
	50–74 y	47–79 y
Gender	70.0% male	35.7% male
Handedness	100.0% right-handed	92.9% right-handed
Age at epilepsy onset M (SD) + range	35.0 (14.6)	-
	15–59 y	
Duration of epilepsy M (SD) + range	22.3 (15.2)	-
	1–50 y	
Type of epilepsy	40.0% cryptogenic localization-related	-
	40.0% symptomatic	
	20.0% idiopathic	
Dominant seizure type [a]	10.0% simple partial	-
	20.0% complex partial	
	20.0% absence	
	0.0% tonic-clonic	
	50.0% seizure free	
Status epilepticus	50.0% yes	
Seizure frequency	50.0% seizure (sz) free	-
	0.0% < 1 sz/y	
	20.0% 1–5 sz/y	
	20.0% 1 sz per 2 months	
	0.0% monthly sz	
	10.0% weekly sz	
	0.0% daily sz	
Drug load [b]	1.5 (0.4)	-
WAIS-IV indexes		
FSIQ	76.7(8.7)*	108.4(13.4)
VCI	94.7 (10.6)	106.2 (12.2)
PRI	75.8 (6.9)*	103.2 (13.8)
WMI	79.6 (10.0)*	104.9 (13.3)
PSI	67.0 (14.4)*	114.6 (8.7)
Deterioration scores[c]		
Det-FSIQ	-22.1 (5.0)*	-1.3 (8.2)
Det-VCI	-0.5 (8.9)	0.2 (6.0)
Det-PRI	-21.0 (4.5)*	0.0 (8.7)
Memory scores		
Auditory	93.9 (9.7)*	109.9 (12.6)
Visual	92.7 (7.0)	102.8 (10.9)
Delayed memory	93.5 (8.4)*	106.3 (10.9)

Note: * = p < 0.01 sign. difference between groups. WMI: Working Memory Index. PSI: Processing Speed Index.

[a] Dominant seizure type is determined for the two years preceding neuropsychological assessment.

[b] The prescribed daily dose of antiepileptic medication divided by the defined daily dose.

[c] The deterioration scores = [WAIS-IV (actual) IQ-scores—OPIE-IV (premorbid) IQ-scores]

preprocessed following the pipeline of [46], using the python script *meica.py* (available at www.bitbucket.org/prantikk/me-ica). Multi-echo- (ME)-ICA cleaning was applied in order to denoise each individual fMRI scan [47]. ME-ICA cleaning has been proven to be the most

robust denoising method for resting-state fMRI, and tend to improve substantially effect sizes and statistical power [48, 49]. Multi-echo cleaned data were further processed using FEAT (FMRI Expert Analysis Tool) Version 6.00, part of FSL (FMRIB's Software Library, www. fmrib.ox.ac.uk/fsl). The following pre-statistics processing was applied; spatial smoothing using a Gaussian kernel of FWHM 5.0mm; grand-mean intensity normalization of the entire 4D dataset by a single multiplicative factor; high-pass temporal filtering (Gaussian-weighted least-squares straight line fitting, with sigma = 50.0 s). The ME-ICA cleaning preprocessing led to an average, among all participant/scans, of 18 activity-related independent components (ICs or networks). Therefore, we chose 18 degrees of freedom for our group-ICA decomposition. The 18 spatial maps corresponding to functional resting-state networks (RSNs) were extracted using group-ICA followed by dual regression as implemented in FSL [50, 51]. After the dual-regression steps, we obtained all subject/session-specific RSN maps and their associated time series. This brain network extraction step is depicted in Fig 2.

After visual inspection and a goodness-of-fit function implementation [52], to match these maps with the RSN template from [11], 4 noise-related RSNs were discarded, and 14 relevant functional brain networks were kept for further analyses. The time series associated with these 14 RSNs were then used to extract our brain networks features as explained in the next section. The 14 networks, or Independent Components (ICs), and their labelling are depicted in Fig 3.

2.2 Static connectivity, causality, phase-coherence and emulative power

First, static functional connectivity (sFC) analysis was performed on all pairs of brain network signals, using Pearson correlation. This is applied for each participant's RSN time series, and each session (RS1 and RS2), leading to two times 24 (14 controls; 10 patients) correlation matrices. The total amount of sFC features per subject/session (unique entries of sFC matrix) was 91 (= 14x13/2; the connectivity matrix being symmetrical, and its diagonal discarded).

Second, using the same ICs (or RSNs) time series we calculated the Granger causality (GC) matrices for each individual and resting-state session using the Matlab toolbox of [53]. A GC connectivity matrix is defined as $G = \{g_{ij}\} \in \mathbb{R}^{N \times N}$ (N = numbers of networks), where each matrix entry g_{ij} represent the directed causal connectivity from network j towards network i. More specifically $g_{ij} = F_{Y \rightarrow X|Z}$, which is the GC between signal Y (time series of network j) and X (time series of network i) conditional on Z (remaining time series of networks $k \neq i \neq j$)— more details in [54]. The upper triangle of G, i.e. $\{g_{ij}\}, \forall j > i$ represent the inward causal pairwise connectivity g_{ij}, while the lower triangle, i.e. $\{g_{ji}\}, \forall i > j$ is all the outward causal connections of $\{g_{ij}\}$. Since GC matrices are asymmetrical (directed connectivity) by subtracting those
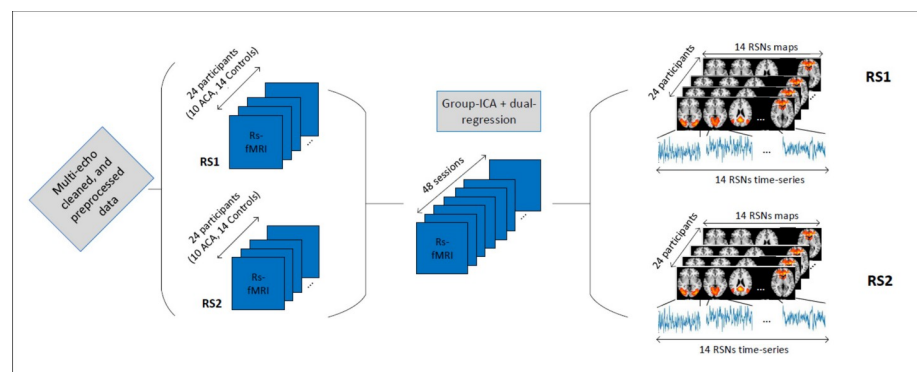

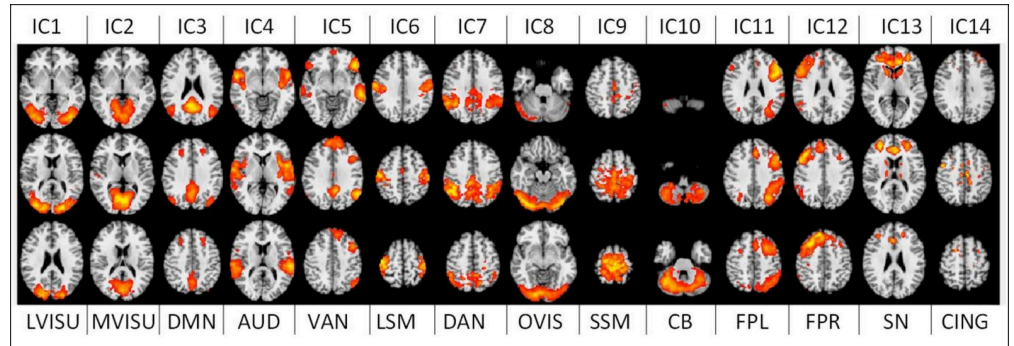**Fig 2. Brain networks (RSN) time series extraction.**

Fig 3. 14 large-scale brain functional resting-state networks (RSNs) used in the study. LVISU–lateral visual network; MVISU–medial visual network; DMN–default mode network; AUD–auditory network; VAN–ventral attention network; LSM—lateral sensory-motor network; DAN–dorsal attention network; OVIS–occipital visual network; SSM–superior sensory-motor network; CB–cerebellar network; FPL–left fronto-parietal network; FPR–right fronto-parietal network; SN–salience network; CING–the cingulate network.

https://doi.org/10.1371/journal.pone.0250222.g003

triangular matrices, i.e lower-upper, we can extract the non-null net pairwise GC triangular matrix $\mathbf{NetGC} = \{netg_{ij}\} = \{g_{ij}—g_{ji}\}, \forall\ i > j$. We also extracted the In- and Out-causal degree of each network by summing respectively the columns and rows of the $\mathbf{G}$ matrices, i.e.

$\mathbf{DegIn} = \{\sum_{j=1}^{N} g_{ij}\} \in \mathbb{R}^{N}$, and $\mathbf{DegOut} = \{\sum_{j=1}^{N} g_{ij}\} \in \mathbb{R}^{N}$. We finally derived the net (out-in) causal degree of each network, i.e. $\mathbf{NetDeg = DegOut—DegIn^{T}}$. Since we have $N = 14$ networks, the total amount of GC features was 315 (= 3x91 (in-, out-, net-GC triangular matrices) + 3x14 (DegIn, DegOut, and NetDeg vectors)). These GC feature matrices and vectors were calculated per subject and session, and are illustrated in Fig 4B.

Thirdly, we applied the wavelet-coherence approach with the following processing steps: (i) extraction of spectro-temporal maps (also called scalograms) of significant phase coherence, i.e. localized (in time and frequency/scales) significant phase-locked correlation between pairs of signals, as in [55]. The phasing between the signals is expressed in radians and extracted from $\theta = arg(Wxy)$ where Wxy is a complex number defining the cross-wavelet transform between the two network signals being assessed. The phase information are summarized in 4 categories: in-phase when $\theta \epsilon (-\pi/4, +\pi/4)$; anti-phase when $\theta \epsilon (3\pi/4, -3\pi/4)$; and signal 1 leading (or lagging) signal 2 when $\theta \epsilon (\pi/4, 3\pi/4)$ (or $\theta \epsilon (-3\pi/4, -\pi/4)$); for simplification we colored the phase information in the wavelet-coherence maps (see Fig 4C). For each of the 5 period scales ([4, 8) s; [8, 16) s; [16, 32) s; [32, 64) s; and [64, 128] s) we extracted the time of coherence (in % of the scan duration) between the 91 pairs of networks. More details on the time of coherence metric in [39]. The time of coherence extraction was performed for all of the 4 aforementioned phases. Therefore, in total we obtained 1820 (= 4x5x91) coherence-based features per subject's session (Fig 4C).

Finally, the Evolutionary Game theory on Network (EGN) was implemented as in [40]. Instead of trying to predict brain signal (time series) dynamics and correlating them to the original BOLD time series, we here simply took the EGN-connectivity matrix $\mathbf{A} = \{a_{ij}\} \in \mathbb{R}^{N \times N}$ ($N =$ numbers of networks), and derived the vectors of emulative powers (EPs). Briefly, each entry of $\mathbf{A}$, a_{ij}, described the pairwise and directed ($i{\rightarrow}j$) weight of the network i in its ability to emulate (positive value, $a_{i,j} > 0$) or not (negative value, $a_{ij} < 0$) the activity of the network j. $\mathbf{A}$ can be seen as similar to the GC connectivity matrices, albeit not in the sense of causality but in terms of replication mechanism. From these matrices of similar size (N^2) as the sFC and GC matrices, we calculated our novel metrics, namely the In-EPs, Out-EPs, and Net-EPs, per participants and session (Fig 4D). The Out-EP of each network, i.e. its power to emulate
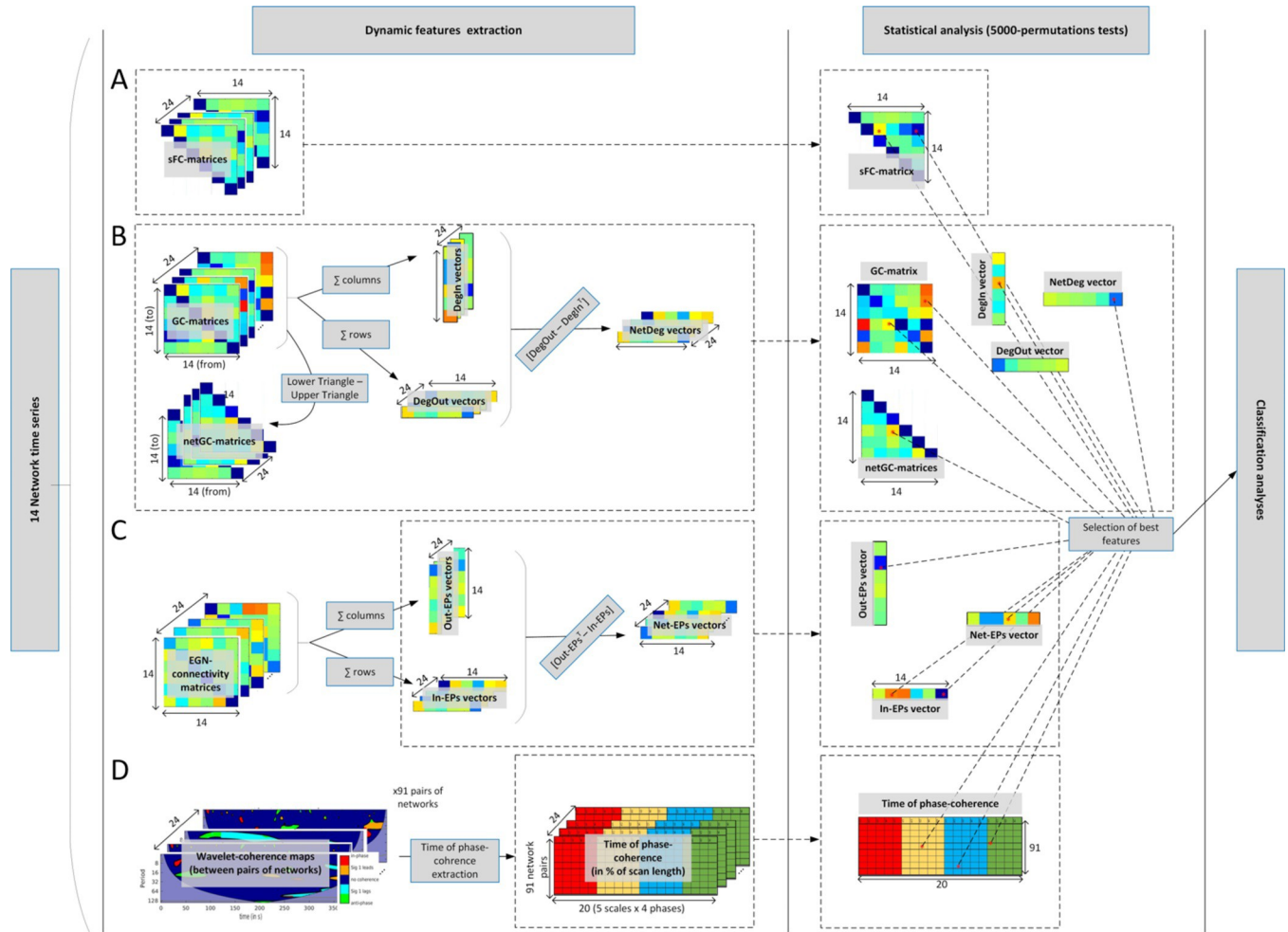
Fig 4. Network feature extraction and statistical analysis. A: extraction of the static functional connectivity features. B: computation of the Granger causality matrices and vectors. C: Emulative power vectors derived from the EGN method; D: Wavelet coherence approach and the time-of-coherence metric extraction.

(replicate) the other networks' activity is calculated by summing the columns of the EGN-connectivity matrix, i.e. $OutEP_i = \sum_{j=1}^{N} a_{ij}$. The power of one network to be emulated by the other networks is represented by its in-EP, that is, the sum of the EGN-connectivity matrix rows, i.e. $InEP_j = \sum_{i=1}^{N} a_{ij}$. And the net replicative power of a network is defined by the Net-EP, i.e. **NetEP = OutEP^T — InEP**. Since $N = 14$, we ended up with three vectors of 14 EPs per person's rs-fMRI session, i.e. 42 features (Fig 4D). The network feature extractions were repeated for the two resting-state sessions.

2.3 Selection of the most relevant features, and classification analysis

After obtaining the subject-/session-specific sFC, GC, time of phase-coherence matrices, and EP vectors, we performed non-parametric permutations tests (5000-permutations) for each entry of the mentioned matrices/vectors. The resulting matrices and vectors were then thresholded at 5% level ($p < 0.05$), giving us the list of pairs of networks where the sFC, GC, time of coherence, and EPs were significantly different between the two groups (ACA and Controls). This statistical analysis was performed to reduce the total number of fMRI-based features to be

used by the classifiers, which was initially 2268 (91 sFC, 315 GC, 1820 WCoh, 42 EGN). This statistical analysis to obtain the best features is depicted in Fig 4.

In order to assess the strength of the abovementioned neurodynamics methods in describing an ACA in patients with epilepsy, classifiers were trained and validated. We used 4 types of machine learning, namely, the support vector machine (SVM), the linear discriminant analysis (LDA), the k-nearest neighborhood (KNN), and the decision tree (DT) algorithms. To validate the classifiers, 5 methods were used: validation on RS2 features (with classifiers trained on RS1's); validation on RS1 features (with classifiers trained on RS2's); leave-on-out cross-validation (LOOCV) in RS1 (24-folds cross-validation); LOOCV in RS2 (24-folds); LOOCV in RS1 and RS2 concatenated (48-folds). 5 validation methods are used to allow us to fully trust the performances of the classifiers. It is also more robust: we can assess consistency and avoid depicting unreproducible 'chance' performances. For each of the classifier types of training and validation, different set-ups of features were used. First, we tested the classifiers using the best features (after statistical analyses) from one type of dynamics at a time, i.e. only best features from sFC analysis, then only significant features from GC analysis, and so on. Next, we refined these set-ups to the use of features that fell into two categories: (i) features/predictors that were used in the DT algorithm, i.e., selected by the Classification And Regression Trees (CART; default split predictor selection technique for classification trees in Matlab); (ii) features that involved the DMN, DAN or SN, since these networks are often mentioned in ageing and cognitive decline literature Then we reiterated refinements of the classifier setups by removing or adding features that still comply with the aforementioned criteria (i and ii), if they were improving classification accuracy in the previous refinement iterations. Such a search for the best combinations of features led us to a dozen of classification analyses per dynamics metrics. Finally, we tested classifiers with combined network features, e.g. using the best GC-based features combined with the best WCoh-based features. We refined the classification models the same way it was performed in the classification analyses per network connectivity metric. We also tried the combination of all best features, i.e. combining all features selected by the statistical analyses of all static and dynamics metrics. In the combined network features setups, a dozen (through refinements) classifiers were also tested. For each of the classifier setup tested (~60 = 5x12), we reported the accuracy, sensitivity and specificity. For clarity, in the Results section, only the best classifiers performances per feature type, and per machine learning algorithms are reported: by looking at the highest average accuracy of the classifiers over the 5 validation methods—mentioned at the beginning of this paragraph.

3 Results

3.1 Selection of the best network features

After extracting all static and dynamic features (sFC, GC, WCoh, EGN), 5000-permutation tests between the two groups' features were applied and thresholded at (uncorrected) p<0.05, giving us the most significant differences between the groups, i.e. the 'best' features. The results of the significant permutation tests for sFC-, GC- and EGN-based features are shown in Supporting Information (S1-S4 Figs in S1 File).

Regarding the WCoh-based features, namely the time-of-coherence measurements, the permutation tests gave us an average of more than 50 significant features per phase (in-phase, anti-phase, leading, and lagging). In order to avoid an overfitting problem, we reduced the number of best features even further, as follows: (i) discarding features that also showed significant differences in controls when comparing RS1 and RS2; (ii) keeping features that showed robustness, i.e. significant in several scales, or in multiple phases; or (iii) time-of-coherence with higher evidence of between-group differences (p<0.01). This led us to having an average

of 10 best features per phase. An example of a pairwise in-phase time-of-coherence that complied with the aforementioned criteria is depicted in Fig 5.

All of the best features for each neurodynamics metric and their labels are summarized in Table 2.

3.2 Classification performances

After static (sFC) and dynamic analyses (GC, WCoh, EGN) followed by the statistical permutation testing we obtained the best descriptors (features) for each metric. All and subsets of these best features were used for training and validating classifiers. In Table 3, the best performances of each individual feature type are shown. For wavelet-coherence, the in-phase time of coherence were the best descriptors of ACA, reaching an average 77.1% accuracy with the decision-tree algorithm, using DMN, SN and visual networks. Using 4 DMN-based and 2 SN-based static connectivity features, the average classification accuracy was 77.9%, with LDA algorithm. With the emulative powers (EGN-based dynamics metric) of the DMN and the DAN we could reach 82.9% accuracy, also using LDA algorithm. Note that the Out-EP and Net-EP of the DAN were not part of selected best features (Table 2), but interestingly improved the classification accuracy when added. This phenomenon can be explained by the fact that, even though Out- and Net-EPs of the DAN are not statistically significant (p>0.05), the way they are pooled with their significant counterparts (In-EPs) in SVM and LDA algorithms, can allow classifiers to be more discriminative. GC-based features, however, led only to 67.9% accuracy with DT algorithm. Overall the metrics giving the best results for classification can be ranked as EPs > sFC > in-phase coherence > GC.

After assessing the best features of each metric, we also trained and tested classifiers with combinations of the features. This gave us the best performances for each classifier type. LDA reached 85% average accuracy using all 86 best features (Table 2). KNN led to an average of 80.8% accuracy with a mix of 82 features that is the 86 best features minus 4 EPs: Out-EPs of DMN and OVIS; and Net-EPs of DMN and CING. DT algorithm reached 80.0% with only 6 features (3 Coherence, 2 EGN, and 1 sFC). And SVM had the best results with 15 features (2 in-phase coherences, 4 in-EPs, 3 GC, and 6 sFC) reaching average accuracy of 90.0%. In the latter SVM set-up, it is worth noting that the independent training and validation, i.e. RS1-trained RS2-validated, and vice-versa, could classify ACA at 91.7% accuracy; the 48-fold LOOCV had 95.8% accuracy. Finally, the overall best average accuracy (81.0%), over all the
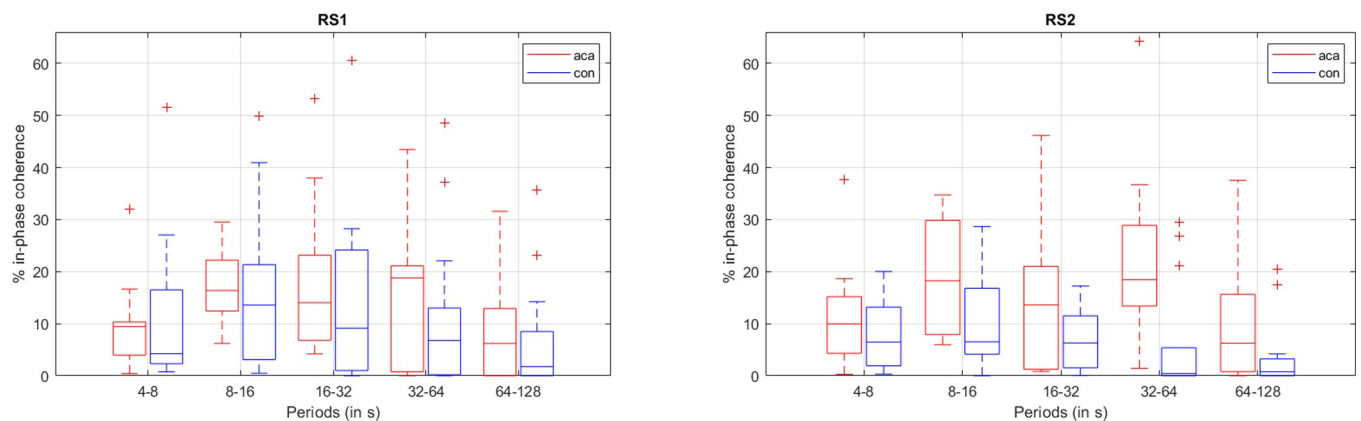

Fig 5. Boxplots of the time of in-phase coherence (in % of scan duration = 7min) for the network pair MVISU-DMN. red boxplot–ACA; blue boxplot–controls; left–RS1; right–RS2. Middle line in the box–median value; box size– 25th to 75th percentiles; whisker limits–most extreme values that are not outliers; '+'–outliers.

Table 2. 86 best features used in the classification analyses.

Wavelet-coherence		Granger-causality		static FC	EGN
in-phase time-of-coherence	*leading time-of-coherence*	*net1→net2 GC*	*net1←net2 GC*	*net1↔net2*	*EPs*
ip_LVISU-OVIS_s1	lead_AUDI-FPR_s1	MVISU->LVISU	MVISU<-LSM	sFC-DMN-VAN	In-EP_DMN
ip_LSM-CING_s1	lead_MVISU-DMN_s1	MVISU->FPL	MVISU<-FPR	sFC-MVISU-DMN	In-EP_DAN
ip_OVIS-SN_s2	lead_MVISU-OVIS_s2	MVISU->CING	LVISU<-AUDI	sFC-DMN-LSM	In-EP_SSM
ip_CB-SN_s2	lead_DMN-OVIS_s2	DMN->AUDI	LVISU<-SSM	sFC-DMN-CB	In-EP_CING
ip_MVISU-DMN_s2	lead_LSM-OVIS_s2	DMN->SN	LVISU<-SN	sFC-AUDI-CING	Out-EP_DMN
ip_OVIS-SN_s3	lead_LSM-OVIS_s3	VAN->CING	VAN<-DAN	sFC-LSM-OVISU	Out-EP_OVIS
ip_CB-SN_s3	lead_OVIS-CB_s3	DAN->FPR	VAN<-AUDI	sFC-DAN-SN	Net-EP_DMN
ip_DMN-DAN_s4	lead_LVISU-VAN_s4	AUDI->SN	DAN<-CING	sFC-OVISU-SN	Net-EP_CING
ip_MVISU-DMN_s4	lead_DMN-VAN_s4	LSM->CING	AUDI<-SSM	sFC-CB-FPL	
anti-phase time-of-coherence	lead_FPL-SN_s4	FPL->FPR	*net pairwise GC*	sFC-CB-CING	
ap_AUDI-FPR_s1	*lagging time-of-coherence*	FPL->CING	netgc_MVISU->LVISU		
ap_VAN-FPL_s1	lag_LVISU-DAN_s1	*network DegIn, DegOut,*	netgc_MVISU->CING		
ap_AUDI-SSM_s1	lag_OVIS-SSM_s1	*and netDeg*	netgc_LVISU->LSM		
ap_DMN-VAN_s2	lag_OVIS-SN_s2	GC_DegOut_LSM	netgc_LVISU->SN		
ap_OVIS-SN_s2	lag_OVIS-FPL_s2	GC_NetDeg_DAN	netgc_DMN->VAN		
ap_LVISU-VAN_s3	lag_CB-FPR_s2	GC_NetDeg_AUDI	netgc_DMN->AUDI		
ap_OVIS-SN_s3	lag_CB-FPL_s2	GC_NetDeg_LSM	netgc_DAN->CING		
ap_VAN-SN_s4	lag_LSM-OVIS_s3		netgc_FPL->FPR		
ap_DMN-AUDI_s5	lag_VAN-CB_s3				

ip–in-phase; ap–anti-phase; lead–leading; lag–lagging; s1 –scale 1 = [4, 8] s; s2 –scale 2 = [8, 16] s; s3 –scale 3 = [16, 32] s; s4 –scale 4 = [32, 64] s; s5 –scale 5 = [64, 128] s;
→(←)–direction of GC; netgc–net pairwise GC (out-in); GC_DegOut–GC out degree of a network; GC_DegIn–GC in degree of a network; sFC–pairwise static
function connectivity; ↔ –bidirectional connectivity for sFC; EGN–evolutionary game theory on network; EPs–emulative powers; In-, Out-, Net-EP–in, out, net
emulative power of a network; net1(2)–network 1 (or 2).

machine-learning algorithms, was obtained using even fewer features (10: 2 in-phase coherence, 2 in-EPs, and 6 sFC). These results are depicted in Table 4. Looking at the classifier algorithms, in general, SVM was performing the best. With few features (< 10), DT was performing quite well, but still not as good as SVM and LDA. KNN was overall the least accurate classification algorithm. It is worth noting that in some set-ups DT algorithm reached 100% accuracy, such as for the LOOCV of RS2 with the mix of 6 features (Table 4); but this was not consistent, since in the same set-up, the RS1-trained-and-RS2-validated classifier reached only 66.7% accuracy.

Overall, EGN-based net emulative powers are the best descriptors, especially when using DMN and DAN features. And when those are combined with specific time of in-phase coherence and static connectivity (correlation) values, SVM algorithm outperforms the other algorithm with an average of 90.0% accuracy; with peaks at 91.7% for the RS-independent training/validation classifications, and 95.8% in the 48-folds LOOCV. For a more intuitive visualization of the results presented above, we graphically summarize Tables 3 and 4 in Fig 6A and 6B respectively.

4 Discussion

4.1 Clinical relevance

We have shown that the emulative powers (Eps) of the default mode network and the dorsal attention networks are biomarkers of ACA. Combining these features with DMN and SN-

Table 3. Summary tables of the best classifier performances for each network connectivity measures: EGN, coherence, sFC, and GC.

	List of feature used		Validation methods	SVM			LDA			KNN			DT		
				acc	sens	spec	acc	sens	spec	acc	sens	spec	acc	sens	spec
EGN	In-EP_DMN		tRS1_vRS2	0.917	0.900	0.929	0.917	0.900	0.929	0.708	0.500	0.857	0.750	0.700	0.786
	In-EP_DAN		tRS2_vRS1	0.708	0.700	0.714	0.833	0.800	0.857	0.708	0.600	0.786	0.583	0.600	0.571
	Out-EP_DMN		Loocv_RS1	0.750	0.700	0.786	0.750	0.700	0.786	0.375	0.300	0.429	0.583	0.600	0.571
	Out-EP_DAN		Loocv_RS2	0.750	0.700	0.786	0.833	0.800	0.857	0.625	0.500	0.714	0.542	0.300	0.714
	Net-EP_DMN		Loocv_conca_RS	0.771	0.750	0.786	0.813	0.750	0.857	0.708	0.600	0.786	0.771	0.700	0.821
	Net-EP_DAN		**Average**	0.779	0.750	0.800	0.829	0.790	0.857	0.625	0.500	0.714	0.646	0.580	0.693
				acc	sens	spec	acc	sens	spec	acc	sens	spec	acc	sens	spec
WCoh			tRS1_vRS2	0.417	1.000	0.000	0.917	0.800	1.000	0.583	0.700	0.500	0.750	1.000	0.571
	ip_OVIS-SN_s2		tRS2_vRS1	0.417	1.000	0.000	0.708	0.700	0.714	0.750	0.900	0.643	0.667	0.500	0.786
	ip_MVISU-DMN_s2		Loocv_RS1	0.417	1.000	0.000	0.417	1.000	0.000	0.625	0.600	0.643	0.708	0.800	0.643
			Loocv_RS2	0.417	1.000	0.000	0.792	0.700	0.857	0.875	0.900	0.857	1.000	1.000	1.000
			Loocv_conca_RS	0.417	1.000	0.000	0.729	0.650	0.786	0.729	0.750	0.714	0.729	0.750	0.714
			Average	0.417	1.000	0.000	0.713	0.770	0.671	0.713	0.770	0.671	0.771	0.810	0.743
				acc	sens	spec	acc	sens	spec	acc	sens	spec	acc	sens	spec
sFC	sFC-DMN-VAN	sFC-DMN-CB	tRS1_vRS2	0.875	0.700	1.000	0.875	0.700	1.000	0.875	0.800	0.929	0.458	0.400	0.500
	sFC-MVISU-DMN	sFC-DAN-SN	tRS2_vRS1	0.750	0.900	0.643	0.792	0.900	0.714	0.750	1.000	0.571	0.542	0.700	0.429
	sFC-DMN-LSM	sFC-OVISU-SN	Loocv_RS1	0.667	0.600	0.714	0.667	0.600	0.714	0.583	0.400	0.714	0.625	0.500	0.714
			Loocv_RS2	0.833	0.700	0.929	0.750	0.600	0.857	0.750	0.500	0.929	0.833	0.700	0.929
			Loocv_conca_RS	0.771	0.700	0.821	0.750	0.700	0.786	0.750	0.550	0.893	0.583	0.500	0.643
			Average	0.779	0.720	0.821	0.767	0.700	0.814	0.742	0.650	0.807	0.608	0.560	0.643
				acc	sens	spec	acc	sens	spec	acc	sens	spec	acc	sens	spec
GC	DMN->AUDI	VAN<-DAN	tRS1_vRS2	0.417	1.000	0.000	0.542	0.300	0.714	0.500	0.200	0.714	0.667	0.400	0.857
	DAN->FPR	VAN<-SN	tRS2_vRS1	0.417	1.000	0.000	0.708	0.700	0.714	0.500	0.400	0.571	0.667	0.600	0.714
	MVISU<-AUDI	FPR<-CB	Loocv_RS1	0.417	1.000	0.000	0.417	1.000	0.000	0.625	0.600	0.643	0.708	0.600	0.786
	MVISU<-FPR	netgc_MVISU->CING	Loocv_RS2	0.417	1.000	0.000	0.458	0.600	0.357	0.542	0.600	0.500	0.750	0.800	0.714
	LVISU<-OVIS	netgc_LVISU->SN	Loocv_conca_RS	0.417	1.000	0.000	0.729	0.700	0.750	0.563	0.500	0.607	0.604	0.550	0.643
	LVISU<-FPR	netgc_DMN->AUDI	**Average**	0.417	1.000	0.000	0.571	0.660	0.507	0.546	0.460	0.607	0.679	0.590	0.743
	OVIS<-AUDI	netgc_FPL->FPR													

Grey highlight–accuracy values; yellow highlight–best averages accuracy in each set-up; blue highlight–accuracy > 80%. SVM–support vector machine; LDA—linear discriminant analyses; KNN—K-nearest neighbours; DT–decision tree. Acc–accuracy; sens–sensitivity; spec–specificity; tRS1(2)_vRS2(1)–trained on RS1(or 2) and validated on RS2 (or 1); Loocv–leave one-out cross-validation; conca_RS–concatenation of RS1 and RS2 features.

related in-phase coherence, and static functional connectivity would allow diagnosing the disorder at an overall 81.0% accuracy (average of all machine-learning algorithms tested). Adding CING- and SSM-related EPs and DAN-, AUDI-, and LSM-related GCs, could even improve SVM accuracy up to 95.8%. This shows the following: (i) dynamics metrics performs better than correlation and causal metrics at classifying an ACA in patients with epilepsy; and (ii) combining them with static functional connectivity improves the classifications. This is in line with a recent meta-analysis on the merit of using dynamic functional connectivity to describe psychological outcomes, especially when performance is assessed with objective measures such as IQ tests—as compared to more subjective (self-reported) psychological assessment—[33].

In the clinical context, the default mode, dorsal attention networks, and the salience network being involved and informative to distinguish neuropsychiatric patients from controls is already shown in previous research. In ageing the DMN and DAN are often mentioned and know to be challenged [56–58]. Also the dynamics in terms of causality is shown to correlate

Table 4. Summary of the best performances of each classifier algorithm: SVM, LDA, KNN, and DT.

	List of features		Validation methods	acc	sens	spec	acc	sens	spec	acc	sens	spec	acc	sens	spec
EGN + WCoh + sFC	ip_OVIS-SN_s2	sFC-DMN-VAN	tRS1_vRS2	0.792	0.500	1.000	0.750	0.600	0.857	0.833	0.800	0.857	0.833	1.000	0.714
	ip_CB-SN_s2	sFC-MVISU-DMN	tRS2_vRS1	0.792	0.600	0.929	0.792	0.900	0.714	0.792	0.800	0.786	0.667	0.500	0.786
	ip_MVISU-DMN_s2	In-EP_DMN	Loocv_RS1	0.833	0.700	0.929	0.833	0.700	0.929	0.833	0.900	0.786	0.750	0.600	0.857
			Loocv_RS2	0.708	0.300	1.000	0.708	0.600	0.786	0.667	0.600	0.714	1.000	1.000	1.000
			Loocv_conca_RS	0.792	0.600	0.929	0.792	0.700	0.857	0.750	0.650	0.821	0.750	0.700	0.786
			Average	0.783	0.540	0.957	0.775	0.700	0.829	0.775	0.750	0.793	0.800	0.760	0.829
				acc	sens	spec	acc	sens	spec	acc	sens	spec	acc	sens	spec
EGN + WCoh + GC + sFC	82 features =	All best features	tRS1_vRS2	0.917	0.800	1.000	0.792	0.600	0.929	0.750	0.800	0.714	0.750	0.400	1.000
		without	tRS2_vRS1	0.917	0.800	1.000	0.833	0.800	0.857	0.833	0.700	0.929	0.667	0.500	0.786
		Out-EP_DMN	Loocv_RS1	0.750	0.700	0.786	0.750	0.700	0.786	0.750	0.700	0.786	0.458	0.300	0.571
		Out-EP_OVIS	Loocv_RS2	0.792	0.700	0.857	0.958	0.900	1.000	0.917	0.800	1.000	0.958	1.000	0.929
		Net-EP_DMN	Loocv_conca_RS	0.938	0.850	1.000	0.833	0.750	0.893	0.792	0.700	0.857	0.542	0.450	0.607
		Net-EP_CING	**Average**	0.863	0.770	0.929	0.833	0.750	0.893	0.808	0.740	0.857	0.675	0.530	0.779
				acc	sens	spec	acc	sens	spec	acc	sens	spec	acc	sens	spec
EGN + WCoh + GC + sFC			tRS1_vRS2	0.750	0.600	0.857	0.792	0.600	0.929	0.750	0.700	0.786	0.750	0.400	1.000
			tRS2_vRS1	0.667	0.800	0.571	0.875	0.800	0.929	0.750	0.700	0.786	0.667	0.500	0.786
	All best 86 features		Loocv_RS1	0.833	0.700	0.929	0.833	0.700	0.929	0.583	0.400	0.714	0.458	0.300	0.571
			Loocv_RS2	0.875	0.800	0.929	0.917	0.800	1.000	0.583	0.400	0.714	0.917	0.900	0.929
			Loocv_conca_RS	0.917	0.800	1.000	0.833	0.750	0.893	0.688	0.500	0.821	0.542	0.450	0.607
			Average	0.808	0.740	0.857	0.850	0.730	0.936	0.671	0.540	0.764	0.667	0.510	0.779
				acc	sens	spec	acc	sens	spec	acc	sens	spec	acc	sens	spec
EGN + WCoh + GC + sFC	ip_MVISU-DMN_s2	sFC-DMN-VAN	tRS1_vRS2	0.917	0.800	1.000	0.917	0.800	1.000	0.708	0.500	0.857	0.708	0.600	0.786
	ip_MVISU-DMN_s4	sFC-MVISU-DMN	tRS2_vRS1	0.917	0.800	1.000	0.583	0.500	0.643	0.708	0.600	0.786	0.667	0.600	0.714
	GC_NetDeg_DAN	sFC-DMN-LSM	Loocv_RS1	0.833	0.700	0.929	0.833	0.700	0.929	0.500	0.300	0.643	0.708	0.600	0.786
	GC_NetDeg_AUDI	sFC-DMN-CB	Loocv_RS2	0.875	0.800	0.929	0.708	0.500	0.857	0.875	0.800	0.929	0.792	0.800	0.786
	GC_NetDeg_LSM	sFC-DAN-SN	Loocv_conca_RS	0.958	0.900	1.000	0.875	0.850	0.893	0.729	0.550	0.857	0.792	0.800	0.786
		sFC-OVISU-SN	**Average**	0.900	0.800	0.971	0.783	0.670	0.864	0.704	0.550	0.814	0.733	0.680	0.771
	In-EP_DMN	In-EP_SSM													
	In-EP_DAN	In-EP_CING													
				acc	sens	spec	acc	sens	spec	acc	sens	spec	acc	sens	spec
EGN + WCoh + sFC	ip_CB-SN_s2	sFC-DMN-VAN	tRS1_vRS2	0.875	0.700	1.000	0.917	0.800	1.000	0.875	0.700	1.000	0.833	1.000	0.714
	ip_MVISU-DMN_s2	sFC-MVISU-DMN	tRS2_vRS1	0.917	0.800	1.000	0.792	0.800	0.786	0.792	0.600	0.929	0.792	0.600	0.929
		sFC-DMN-LSM	Loocv_RS1	0.750	0.500	0.929	0.750	0.500	0.929	0.625	0.700	0.571	0.792	0.700	0.857
	In_EP_DMN	sFC-DMN-CB	Loocv_RS2	0.875	0.800	0.929	0.708	0.500	0.857	0.792	0.700	0.857	0.667	0.500	0.786
	In-EP_DAN	sFC-DAN-SN	Loocv_conca_RS	0.917	0.800	1.000	0.875	0.850	0.893	0.854	0.750	0.929	0.813	0.700	0.893
		sFC-OVISU-SN	**Average**	0.867	0.720	0.971	0.808	0.690	0.893	0.788	0.690	0.857	0.779	0.700	0.836
		overall average =													
			0.810												

Grey highlight–accuracy values; yellow highlight–best averages accuracy in each set-up; blue highlight–accuracy > 80%. SVM–support vector machine; LDA—linear discriminant analyses; KNN—K-nearest neighbours; DT–decision tree. Acc–accuracy; sens–sensitivity; spec–specificity; tRS1(2)_vRS2(1)–trained on RS1 (or 2) and validated on RS2(or 1); Loocv–leave one-out cross-validation; conca_RS–concatenation of RS1 and RS2 features.

with psychological performances [28]. Static and dynamic functional connectivity of the DMN and DAN might be explained by the compensatory mechanism observed in aging, as described in the CRUNCH model [59, 60]. This compensatory mechanism is defined as the cognitive reserve in the study of [61] wherein DMN and DAN are also involved. Other studies have
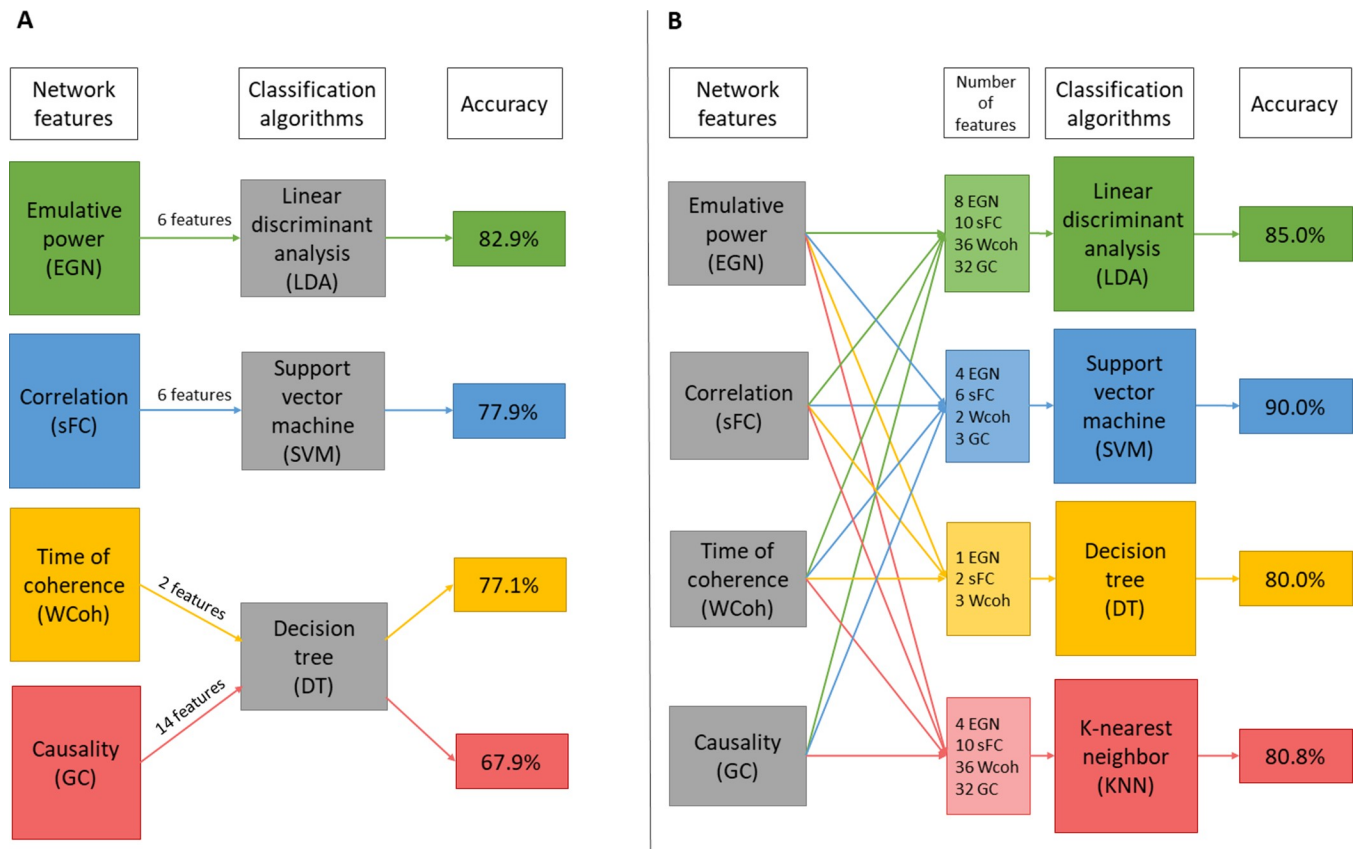
Fig 6. Graphical summary of the classification results. A: best performances of each network connectivity metric. B: best performances of each classifier algorithm.

linked cognitive decline with changes in static and dynamic functional connectivity between the DMN and DAN [56, 62, 63]. The salience network (SN), which was part of our sFC best features, and its overall decreased in functional connectivity, is also a marker of brain ageing [57, 59]. SN has also a pivotal role in predicting age and cognitive performances (ranging from episodic memory to executive functions), in healthy elderly with cognitive decline [64]. Regarding mild cognitive impairment, which is a disorder wherein symptoms resemble the deficit in ACA patients, the sFC showed also disturbed network activity in the aforementioned brain regions [27, 65]. Finally in a review paper, from 81 fMRI studies where elderly had a significant cognitive decline, 50% of the studies showed changes in brain activation occurring in the DAN, and 15.3% in the DMN [66].

Sensorimotor networks are also implicated in the process of cognitive ageing [67]. That explains the involvement of the LSM-DMN sFC, the Net GC degree of the LSM, and the In-EP of the SSM, in our best classifier set-up. Finally, the time of in-phase coherence between the pair MVISU-DMN often helped the performances of our classifiers. This might be explained by the anterior-posterior shift observed in ageing in the PASA model of the ageing brain [68]. This shift involved an over-recruitment of the posterior brain functional network (here DMN-MVISU connectivity) in order to compensate for the 'normal' decline in ageing of the visual abilities. And this correlates negatively with the cognitive performances, similar to the increase of in-phase coherence in ACA patients with deterioration in IQ.

ACA patient suffers more specifically from a deterioration in fluid intelligence, which is described as the ability to think logically and solve problems with a limited amount of task-related information [69]. The aforementioned DMN, CING (for cognitive control), and sensorimotor (LSM/SSM) networks have been shown to be linked to this type of intelligence/cognitive processing [70]. The fluid intelligence might come from the ability to switch from perceptive network to processing network, and the ability to switch and hold attention. The DMN, SN and DAN are the 3 networks involved in self-referential processes, dynamic switching between rest and task, and the voluntary allocation of attention [71–73]. Having less copying mechanism here (as shown by the EGN dynamics) in those networks, might reflect a more rigid brain processing, i.e. less fluidic integration, which might explain the poor results in Perceptual Reasoning Index (PRI; fluid intelligence test).

Overall, the DMN, DAN, SN and their dynamic and static functional connectivity to multiple sensory-related networks (visual, sensorimotor) could, no matter the resting-state, help classify correctly patients from healthy subjects. And the involvement of these networks are in line with current research on cognitive decline in ageing, and brain functional connectivity [28, 29, 59, 62, 64, 66, 74, 75].

4.2 Technical insights

Evolutionary game theory on networks and its derived emulative powers were the best at describing ACA (highest classifying performances) as compared to the other metrics used in this study. More specifically the In-emulative power of the DMN and DAN were strong biomarkers of ACA. In general, for RS1 and RS2, the DMN In-EPs of the patients were negative, whereas those of the controls, positive. This shows that patients' DMN tends to have a non-emulative (non-replicative) attitude, i.e., all other networks do not tend to copy the DMN activity. For the DAN both groups showed negative in-EPs (non-emulative attitude), but with stronger negative power in ACA patients. The involvement of those networks make sense as seen in the previous paragraph on the clinical relevance. However, the rational for why this novel dynamics metric show stronger discriminatory power as compare to, say, the In or Out-degree of Granger-causality of the DMN and DAN remains unclear. It is indeed difficult to conceive that the replication mechanism between signals do not equate to some degree to a correlation (for sFC) or causal (with GC) effect. In a side study, we actually tried to find similitude between EPs and Deg. GC, which gave us non-significant correlation (between the two metric values). A hypothesis is that, since EGN model is based on differential equations, the emulative values between the networks are influencing not by the network signal directly, but rather by their rate of change in activity ($\frac{dx(t)}{dt}$; where $x(t)$ = RSN activity signal). More details about the EGN model, and its replicator dynamics, in [40].

Regarding SVM and LDA approaches, their ranking in our study is in line with the way these algorithms work. Indeed, in a setup with features having co-variability, and normally distributed, LDA will perform better, with is shown when using many of our most relevant features, and trying to find overall separable (with all of the features) means/centroids. On the contrary SVM, which considers all training data points to find the values (vectors) that help to maximize margin between pools of features, is more robust to outliers—which are clearly present in our small dataset. However, we can expect that with a larger multi-dimensional dataset, the two algorithms (LDA and SVM) would not have substantial differences in performance. In order to increase their performances, a solution might be to combine the two algorithms [76, 77]. The decision tree algorithm is attractive in its simplicity: sequential splitting of the features with thresholds, but might be too dependent on the training sample—as shown by our strong variance in classification accuracy over the 5 validation methods. Regarding KNN, a more

thorough testing with different K values might have been of benefit. Other type of classifier such as elastic net, logistic regression, or naïve Bayes classifier could possibly be applied as well. However, they have shown in general a substantial lower power at classifying neuropsychiatric disorders, as seen in the summary tables of [78].

Finally, for all classifiers presented here, the Matlab default set-ups of each of the machine learning algorithm were used. We only tried, on our best SVM classifiers, to change the kernel, from Gaussian to polynomial; but this had given us less accurate results. More hyper-parameter optimization could be investigated. Also, the worst—but simplest to explain—algorithm, namely decision tree (best at 80%, using only 6 features, with GC), could further be optimized. For instance, by changing node splitting rules from an ascending impurity gain (of Gini's Diversity Index) to descending one; or by changing directly the predictor selections (which features are used in the nodes of the tree) with curvature tests, or interaction tests.

However, since the results are quite robust in SVM, the first step might be to reproduce the results with new (unseen) data, and see if these classifiers continue to provide high performances. Other neuropsychiatric disorders could also be tested with the same pipeline. E.g. autism could be investigated using the rs-fMRI datasets of ABIDE repository (http://fcon_1000.projects.nitrc.org/indi/abide/). With such a large dataset, the reliability of the accuracy obtained using our pipeline is much greater, and the optimisation would be more worthy.

As mentioned in the introduction, a few fMRI research attempt similar classification of neuropsychiatric disorders using more advanced machine learning algorithms, such as convolutional neural networks, or deep auto-encoder [79, 80]. The added value is that those algorithms can be used not only in the supervised multi-labels classification process, but also directly in an unsupervised feature extraction. Though, an important drawback of these advanced classification techniques is that they usually need an important amount of data to be trained upon, which are often not available in case of rs-fMRI data of neuropsychiatric disorders. Also, the understanding and explanation of the feature maps obtained at different CNN layers can be arduous more computationally intensive and troublesome to be clearly explained and descriptive.

Even though research in advance AI for psychoradiology seems promising in many fields, especially segmentation and auto-labelling of cancer or lesion for instance, common machine learning algorithms such as LDA or SVM make the results more understandable and explainable for the clinicians, radiologists and ultimately the patients. For instance, the linear combination of static and dynamic functional connectivity between a handful of well-described networks, can be easily display, and showing how the algorithm split the populations (patients vs controls) is readily feasible. Such simple design and visualization of the process make possible targetable treatment that must be less complicated to design. And following the evolution of such dynamic or static fMRI-based brain features is rather simple, and thus can greatly help to refine classification models to a prognostic level; or to assess lasting effects of different treatments of psychiatric disorders.

4.3 Limitations

There are several limitations in this study. First, as mentioned in the previous paragraph, the study would benefit from a larger dataset. Testing the classifiers on new and unseen data extracted from another scanner (different parameters, e.g. TR or duration of the rs-fMRI), and from another site (different medical centre, or country) would also provide insight regarding the robustness of the methods and the features presented here. However, gathering more fMRI data from ACA patients is not an easy task, since this epilepsy co-morbidity is only recently described, and acquiring systematic rs-fMRI data from elderly patients with epilepsy is not

common practise yet. Moreover, having a bigger in-house dataset of participants would not mean getting lower performances, but rather more stable. Indeed, it has been proven by testing pools of data of different sizes, that the accuracy of SVM classification gets simply more reliable less variability in performances as the training sample size increases, in case of data from schizophrenic patients acquired with the same protocol [81]. Nevertheless, the cross-center robustness still needs to be tested.

Second, with high performances of binary classification, we showed a strong diagnostic power of the dynamics features. However, the ACA patients were already diagnosed with ACA based on a clear loss of fluid IQ after psychological assessment. Hence, having an automated tool that diagnoses ACA with lower accuracy than diagnoses based on psychological tests are not needed. In that regards, our goal was not to show the highest performance, but to rank the dynamics features, and show the benefit of combining different dynamic features, using solely rs-fMRI data. Also, with refinement, this analysis could extrapolate from the two class (binary) classification/diagnosis to a multi-class separation, and show prognostic power, for example in order to predict mental ages, or rate of decline in intelligence of patients with ACA (based on a stratified approach, through severity of the ACA for instance).

Despite those limitations, we are confident that the emulative powers, and the times of in-phase coherence of large-scale resting-state networks are informative descriptors of neuropsy-chiatric disorders, and that combining them with known metrics such as sFC and GC can lead to accurate diagnoses. One could expect similar performance, when testing the new metrics upon schizophrenic, autistic, or depressive patients for example. And this pipeline to train data and validate clinical diagnoses of (neuro)psychiatric disorders can be of great help in clinics and contribute to the field of psychoradiology [82].

5 Conclusions

We presented a novel metric for neurodynamics extracted from the evolutionary game theory on network approach: The emulative power of brain networks, i.e. the propensity of a network for replicating another network activity. The emulative powers of the default mode network and dorsal attention network seem defective in ACA; and using these features combined with in-phase coherence measurements, and static functional connectivity yield to an average diag-nostic accuracy of 90%, using the SVM algorithm. With regard to the field of neuropsychora-diology, other neuropsychiatric disorders could be tested using similar fMRI-based dynamics features, and could lead to better understanding, and subsequently better treatments of mental disorders. Also, with refinements of the models and the classification pipeline, we could envis-age that the fMRI-based neurodynamics presented here would have a prognostic value, for example if labels are not simply binary (stratified models), other feature types are added (mul-timodal approaches), and using cohort study design (longitudinal cross-sectional studies). This pipeline applied on larger datasets, and if replicated, would demonstrate robustness of these new neurodynamics metrics and reliability of the methods, and hence could be to some extent clinically used.

Supporting information

S1 File.
(PDF)

S1 Data. Network time series (.mat) and network images.
(ZIP)

Author Contributions

Conceptualization: Antoine Bernas.

Data curation: Antoine Bernas, Lisanne E. M. Breuer.

Formal analysis: Antoine Bernas.

Investigation: Antoine Bernas, Lisanne E. M. Breuer.

Methodology: Antoine Bernas, Svitlana Zinger.

Project administration: Albert P. Aldenkamp.

Supervision: Albert P. Aldenkamp, Svitlana Zinger.

Validation: Albert P. Aldenkamp, Svitlana Zinger.

Visualization: Antoine Bernas.

Writing – original draft: Antoine Bernas.

Writing – review & editing: Albert P. Aldenkamp, Svitlana Zinger.

References

1. Helmstaedter C, Aldenkamp AP, Baker GA, Mazarati A, Ryvlin P, Sankar R. Disentangling the relationship between epilepsy and its behavioral comorbidities—The need for prospective studies in new-onset epilepsies. Epilepsy Behav. 2014; 31: 43–47. https://doi.org/10.1016/j.yebeh.2013.11.010 PMID: 24333577

2. Besseling RMH, Jansen JFA, Overvliet GM, Van Der Kruijs SJM, Vles JSH, Ebus SCM, et al. Reduced functional integration of the sensorimotor and language network in rolandic epilepsy. NeuroImage Clin. 2013; 2: 239–246. https://doi.org/10.1016/j.nicl.2013.01.004 PMID: 24179777

3. Braakman HMH, Vaessen MJ, Jansen JFA, Debeij-Van Hall MHJA, De Louw A, Hofman PAM, et al. Frontal lobe connectivity and cognitive impairment in pediatric frontal lobe epilepsy. Epilepsia. 2013; 54: 446–454. https://doi.org/10.1111/epi.12044 PMID: 23253092

4. Hermann B, Seidenberg M, Sager M, Carlsson C, Gidal B, Sheth R, et al. Growing old with epilepsy: the neglected issue of cognitive and brain health in aging and elder persons with chronic epilepsy. Epilepsia. 2008; 49: 731–40. https://doi.org/10.1111/j.1528-1167.2007.01435.x PMID: 18031544

5. Helmstaedter C, Elger CE. Chronic temporal lobe epilepsy: A neurodevelopmental or progressively dementing disease. Brain. 2009; 132: 2822–2830. https://doi.org/10.1093/brain/awp182 PMID: 19635728

6. Sen A, Capelli V, Husain M. Cognition and dementia in older patients with epilepsy. Brain. 2018; 141: 1592–1608. https://doi.org/10.1093/brain/awy022 PMID: 29506031

7. Breuer LEM, Boon P, Bergmans JWM, Mess WH, Besseling RMH, de Louw A, et al. Cognitive deterioration in adult epilepsy: Does accelerated cognitive ageing exist? Neurosci Biobehav Rev. 2016; 64: 1–11. https://doi.org/10.1016/j.neubiorev.2016.02.004 PMID: 26900650

8. Breuer LEM, Carrette ECB, Boon P, Bernas A, Besseling RMH, Aldenkamp AP, et al. Accelerated Cognitive Ageing in Epilepsy: A Neuropsychological Evaluation of Cognitive Deterioration. Arch Clin Neuropsychol. 2019. https://doi.org/10.1093/arclin/acy042 PMID: 29718070

9. van den Heuvel MP, Hulshoff Pol HE. Exploring the brain network: A review on resting-state fMRI functional connectivity. Eur Neuropsychopharmacol. 2010; 20: 519–534. https://doi.org/10.1016/j.euroneuro.2010.03.008 PMID: 20471808

10. Power JD, Cohen AL, Nelson SM, Wig GS, Barnes KA, Church JA, et al. Functional Network Organization of the Human Brain. Neuron. 2011; 72: 665–678. https://doi.org/10.1016/j.neuron.2011.09.006 PMID: 22099467

11. Smith SM, Fox PT, Miller KL, Glahn DC, Fox PM, Mackay CE, et al. Correspondence of the brain's functional architecture during activation and rest. Proc Natl Acad Sci U S A. 2009; 106: 13040–5. https://doi.org/10.1073/pnas.0905267106 PMID: 19620724

12. Cole DM, Smith SM, Beckmann CF. Advances and pitfalls in the analysis and interpretation of resting-state FMRI data. Front Syst Neurosci. 2010; 4: 8. https://doi.org/10.3389/fnsys.2010.00008 PMID: 20407579

13. Nomi JS, Uddin LQ. Developmental changes in large-scale network connectivity in autism. NeuroImage Clin. 2015; 7: 732–741. https://doi.org/10.1016/j.nicl.2015.02.024 PMID: 25844325

14. Laird AR, Fox PM, Eickhoff SB, Turner JA, Ray KL, McKay DR, et al. Behavioral Interpretations of Intrinsic Connectivity Networks. J Cogn Neurosci. 2011; 23: 4022–4037. https://doi.org/10.1162/jocn_a_00077 PMID: 21671731

15. Choe AS, Jones CK, Joel SE, Muschelli J, Belegu V, Caffo BS, et al. Reproducibility and temporal structure in weekly resting-state fMRI over a period of 3.5 years. PLoS One. 2015; 10: 1–29. https://doi.org/10.1371/journal.pone.0140134 PMID: 26517540

16. Beckmann CF, DeLuca M, Devlin JT, Smith SM. Investigations into resting-state connectivity using independent component analysis. Philos Trans R Soc Lond B Biol Sci. 2005; 360: 1001–13. https://doi.org/10.1098/rstb.2005.1634 PMID: 16087444

17. Hull J V., Jacokes ZJ, Torgerson CM, Irimia A, Van Horn JD, Aylward E, et al. Resting-state functional connectivity in autism spectrum disorders: A review. Front Psychiatry. 2017;7. https://doi.org/10.3389/fpsyt.2017.00007 PMID: 28210230

18. Müller RA, Shih P, Keehn B, Deyoe JR, Leyden KM, Shukla DK. Underconnected, but how? A survey of functional connectivity MRI studies in autism spectrum disorders. Cereb Cortex. 2011; 21: 2233–2243. https://doi.org/10.1093/cercor/bhq296 PMID: 21378114

19. Park B, Kim J, Park H. Differences in connectivity patterns between child and adolescent attention deficit hyperactivity disorder patients. 2016 38th Annual International Conference of the IEEE Engineering in Medicine and Biology Society (EMBC). IEEE; 2016. pp. 1127–1130. https://doi.org/10.1109/EMBC.2016.7590902

20. Zang YF, Yong H, Chao-Zhe Z, Qing-Jiu C, Man-Qiu S, Meng L, et al. Altered baseline brain activity in children with ADHD revealed by resting-state functional MRI. Brain Dev. 2007; 29: 83–91. https://doi.org/10.1016/j.braindev.2006.07.002 PMID: 16919409

21. Kaiser RH, Whitfield-Gabrieli S, Dillon DG, Goer F, Beltzer M, Minkel J, et al. Dynamic Resting-State Functional Connectivity in Major Depression. Neuropsychopharmacology. 2016; 41: 1822–1830. https://doi.org/10.1038/npp.2015.352 PMID: 26632990

22. Rashid B, Damaraju E, Pearlson GD, Calhoun VD. Dynamic connectivity states estimated from resting fMRI Identify differences among Schizophrenia, bipolar disorder, and healthy control subjects. Front Hum Neurosci. 2014; 8: 1–13. https://doi.org/10.3389/fnhum.2014.00001 PMID: 24474914

23. Friston KJ. Functional and Effective Connectivity: A Review. Brain Connect. 2011; 1: 13–36. https://doi.org/10.1089/brain.2011.0008 PMID: 22432952

24. Friston K, Moran R, Seth AK. Analysing connectivity with Granger causality and dynamic causal modelling. Curr Opin Neurobiol. 2013; 23: 172–178. https://doi.org/10.1016/j.conb.2012.11.010 PMID: 23265964

25. Bernas A, Barendse EM, Aldenkamp AP, Backes WH, Hofman PAM, Hendriks MPH, et al. Brain resting-state networks in adolescents with high-functioning autism: Analysis of spatial connectivity and temporal neurodynamics. Brain Behav. 2018; e00878. https://doi.org/10.1002/brb3.878 PMID: 29484255

26. Rolls ET, Cheng W, Gilson M, Qiu J, Hu Z, Ruan H, et al. Effective Connectivity in Depression. Biol Psychiatry Cogn Neurosci Neuroimaging. 2018; 3: 187–197. https://doi.org/10.1016/j.bpsc.2017.10.004 PMID: 29529414

27. Zhenyu Liu, Lijun Bai, Ruwei Dai, Chongguang Zhong, Hu Wang, Youbo You, et al. Exploring the effective connectivity of resting state networks in Mild Cognitive Impairment: An fMRI study combining ICA and multivariate Granger causality analysis. 34th Annual International Conference of the IEEE Engineering in Medicine and Biology Society. IEEE; 2012. pp. 5454–5457. https://doi.org/10.1109/EMBC.2012.6347228

28. Tsvetanov KA, Henson RNA, Tyler LK, Razi A, Geerligs L, Ham TE, et al. Extrinsic and Intrinsic Brain Network Connectivity Maintains Cognition across the Lifespan Despite Accelerated Decay of Regional Brain Activation. J Neurosci. 2016; 36: 3115–3126. https://doi.org/10.1523/JNEUROSCI.2733-15.2016 PMID: 26985024

29. Chand G, Wu J, Hajjar I, Qiu D. Interactions of the salience network and its subsystems with the default-mode and the central-executive networks in normal aging and mild cognitive impairment. Brain Connect. 2017;7: brain.2017.0509. https://doi.org/10.1089/brain.2017.0509 PMID: 28707959

30. Damaraju E, Allen EA, Belger A, Ford JM, McEwen S, Mathalon DH, et al. Dynamic functional connectivity analysis reveals transient states of dysconnectivity in schizophrenia. NeuroImage Clin. 2014; 5: 298–308. https://doi.org/10.1016/j.nicl.2014.07.003 PMID: 25161896

31. Di X, Biswal BB. Dynamic brain functional connectivity modulated by resting-state networks. Brain Struct Funct. 2013; 220: 37–46. https://doi.org/10.1007/s00429-013-0634-3 PMID: 25713839

32. Li C, Xia L, Ma J, Li S, Liang S, Ma X, et al. Dynamic functional abnormalities in generalized anxiety disorders and their increased network segregation of a hyperarousal brain state modulated by insomnia. J Affect Disord. 2019; 246: 338–345. https://doi.org/10.1016/j.jad.2018.12.079 PMID: 30597294

33. Liégeois R, Li J, Kong R, Orban C, Van De Ville D, Ge T, et al. Resting brain dynamics at different time-scales capture distinct aspects of human behavior. Nat Commun. 2019; 10: 2317. https://doi.org/10.1038/s41467-019-10317-7 PMID: 31127095

34. Calhoun VD, Miller R, Pearlson G, Adali T. The Chronnectome: Time-Varying Connectivity Networks as the Next Frontier in fMRI Data Discovery. Neuron. 2014; 84: 262–274. https://doi.org/10.1016/j.neuron.2014.10.015 PMID: 25374354

35. Shakil S, Lee CH, Keilholz SD. Evaluation of sliding window correlation performance for characterizing dynamic functional connectivity and brain states. Neuroimage. 2016; 133: 111–128. https://doi.org/10.1016/j.neuroimage.2016.02.074 PMID: 26952197

36. Hindriks R, Adhikari MH, Murayama Y, Ganzetti M, Mantini D, Logothetis NK, et al. Can sliding-window correlations reveal dynamic functional connectivity in resting-state fMRI? Neuroimage. 2016; 127: 242–256. https://doi.org/10.1016/j.neuroimage.2015.11.055 PMID: 26631813

37. Rashid B, Arbabshirani MR, Damaraju E, Cetin MS, Miller R, Pearlson GD, et al. Classification of schizophrenia and bipolar patients using static and dynamic resting-state fMRI brain connectivity. Neuroimage. 2016; 134: 645–657. https://doi.org/10.1016/j.neuroimage.2016.04.051 PMID: 27118088

38. Chang C, Glover GH. Time–frequency dynamics of resting-state brain connectivity measured with fMRI. Neuroimage. 2010; 50: 81–98. https://doi.org/10.1016/j.neuroimage.2009.12.011 PMID: 20006716

39. Bernas A, Aldenkamp AP, Zinger S. Wavelet coherence-based classifier: A resting-state functional MRI study on neurodynamics in adolescents with high-functioning autism. Comput Methods Programs Biomed. 2018; 154: 143–151. https://doi.org/10.1016/j.cmpb.2017.11.017 PMID: 29249338

40. Madeo D, Talarico A, Pascual-Leone A, Mocenni C, Santarnecchi E. An Evolutionary Game Theory Model of Spontaneous Brain Functioning. Sci Rep. 2017; 7: 15978. https://doi.org/10.1038/s41598-017-15865-w PMID: 29167478

41. Ktena SI, Parisot S, Ferrante E, Rajchl M, Lee M, Glocker B, et al. Metric learning with spectral graph convolutions on brain connectivity networks. Neuroimage. 2018; 169: 431–442. https://doi.org/10.1016/j.neuroimage.2017.12.052 PMID: 29278772

42. Deshpande G, Wang P, Rangaprakash D, Wilamowski B. Fully connected cascade artificial neural network architecture for attention deficit hyperactivity disorder classification from functional magnetic resonance imaging data. IEEE Trans Cybern. 2015; 45: 2668–2679. https://doi.org/10.1109/TCYB.2014.2379621 PMID: 25576588

43. Kim J, Calhoun VD, Shim E, Lee JH. Deep neural network with weight sparsity control and pre-training extracts hierarchical features and enhances classification performance: Evidence from whole-brain resting-state functional connectivity patterns of schizophrenia. Neuroimage. 2016; 124: 127–146. https://doi.org/10.1016/j.neuroimage.2015.05.018 PMID: 25987366

44. Holdnack JA, Schoenberg MR, Lange RT, Iverson GL. Predicting Premorbid Ability for WAIS-IV, WMS-IV and WASI-II. WAIS-IV, WMS-IV, and ACS: Advanced Clinical Interpretation. Elsevier Inc.; 2013. https://doi.org/10.1080/09297049.2012.705822 PMID: 22775769

45. Wechsler D. WAIS-IV: Wechsler adult intelligence scale. San Antonio, TX: Psychological Corporation. 2008. https://doi.org/10.1016/S0043-1354(02)00019-2

46. Kundu P, Inati SJ, Evans JW, Luh W, Bandettini PA. Differentiating BOLD and non-BOLD signals in fMRI time series using multi-echo EPI. Neuroimage. 2012; 60: 1759–1770. https://doi.org/10.1016/j.neuroimage.2011.12.028 PMID: 22209809

47. Kundu P, Voon V, Balchandani P, Lombardo M V., Poser BA, Bandettini P. Multi-Echo fMRI: A Review of Applications in fMRI Denoising and Analysis of BOLD Signals. Neuroimage. 2017; 1–22. https://doi.org/10.1016/j.neuroimage.2017.03.033 PMID: 28363836

48. Dipasquale O, Sethi A, Laganà MM, Baglio F, Baselli G, Kundu P, et al. Comparing resting state fMRI de-noising approaches using multi- and single-echo acquisitions. PLoS One. 2017; 12: e0173289. https://doi.org/10.1371/journal.pone.0173289 PMID: 28323821

49. Lombardo M V., Auyeung B, Holt RJ, Waldman J, Ruigrok AN V, Mooney N, et al. Improving effect size estimation and statistical power with multi-echo fMRI and its impact on understanding the neural systems supporting mentalizing. Neuroimage. 2016; 142: 55–66. https://doi.org/10.1016/j.neuroimage.2016.07.022 PMID: 27417345

50. Beckmann CF, Mackay CE, Filippini N, Smith SM. Group comparison of resting-state FMRI data using multi-subject ICA and dual regression. Human Brain Mapping Conference. 2009. p. 181. Available: http://fsl.fmrib.ox.ac.uk/analysis/dualreg/dualreg_poster.pdf

51. Filippini N, MacIntosh BJ, Hough MG, Goodwin GM, Frisoni GB, Smith SM, et al. Distinct patterns of brain activity in young carriers of the APOE-epsilon4 allele. Pnas. 2009; 106: 7209–7214. https://doi.org/10.1073/pnas.0811879106 PMID: 19357304

52. Greicius MD, Srivastava G, Reiss AL, Menon V. Default-mode network activity distinguishes Alzheimer's disease from healthy aging: evidence from functional MRI. Proc Natl Acad Sci U S A. 2004; 101: 4637–4642. https://doi.org/10.1073/pnas.0308627101 PMID: 15070770

53. Barnett L, Seth AK. The MVGC multivariate Granger causality toolbox: A new approach to Granger-causal inference. J Neurosci Methods. 2014; 223: 50–68. https://doi.org/10.1016/j.jneumeth.2013.10.018 PMID: 24200508

54. Bressler SL, Seth AK. Wiener–Granger Causality: A well established methodology. Neuroimage. 2011; 58: 323–329. https://doi.org/10.1016/j.neuroimage.2010.02.059 PMID: 20202481

55. Grinsted A, Moore JC, Jevrejeva S. Application of the cross wavelet transform and wavelet coherence to geophysical time series. Nonlinear Process Geophys. 2004; 11: 561–566. https://doi.org/10.5194/npg-11-561-2004

56. Damoiseaux JS, Beckmann CF, Arigita EJS, Barkhof F, Scheltens P, Stam CJ, et al. Reduced resting-state brain activity in the "default network" in normal aging. Cereb Cortex. 2008; 18: 1856–1864. https://doi.org/10.1093/cercor/bhm207 PMID: 18063564

57. Onoda K, Ishihara M, Yamaguchi S. Decreased Functional Connectivity by Aging Is Associated with Cognitive Decline. J Cogn Neurosci. 2012; 24: 2186–2198. https://doi.org/10.1162/jocn_a_00269 PMID: 22784277

58. Ferreira LK, Regina ACB, Kovacevic N, Martin MDGM, Santos PP, Carneiro CDG, et al. Aging effects on whole-brain functional connectivity in adults free of cognitive and psychiatric disorders. Cereb Cortex. 2016; 26: 3851–3865. https://doi.org/10.1093/cercor/bhv190 PMID: 26315689

59. Sala-Llonch R, Bartrés-Faz D, Junqué C. Reorganization of brain networks in aging: a review of functional connectivity studies. Front Psychol. 2015; 6: 663. https://doi.org/10.3389/fpsyg.2015.00663 PMID: 26052298

60. Reuter-Lorenz PA, Cappell KA. Neurocognitive aging and the compensation hypothesis. Curr Dir Psychol Sci. 2008; 17: 177–182. https://doi.org/10.1111/j.1467-8721.2008.00570.x

61. Bastin C, Yakushev I, Bahri MA, Fellgiebel A, Eustache F, Landeau B, et al. Cognitive reserve impacts on inter-individual variability in resting-state cerebral metabolism in normal aging. Neuroimage. 2012; 63: 713–722. https://doi.org/10.1016/j.neuroimage.2012.06.074 PMID: 22796505

62. Tomasi D, Volkow ND. Aging and functional brain networks. Mol Psychiatry. 2012; 17: 549–558. https://doi.org/10.1038/mp.2011.81 PMID: 21727896

63. Onoda K, Ishihara M, Yamaguchi S. Aging effects on functional connectivity within and between resting-state networks. 2012 ICME Int Conf Complex Med Eng C 2012 Proc. 2012;8: 119–124. https://doi.org/10.1109/ICCME.2012.6275599

64. La Corte V, Sperduti M, Malherbe C, Vialatte F, Lion S, Gallarda T, et al. Cognitive Decline and Reorganization of Functional Connectivity in Healthy Aging: The Pivotal Role of the Salience Network in the Prediction of Age and Cognitive Performances. Front Aging Neurosci. 2016; 8: 1–12. https://doi.org/10.3389/fnagi.2016.00001 PMID: 26858637

65. Farràs-Permanyer L, Guàrdia-Olmos J, Peró-Cebollero M. Mild cognitive impairment and fMRI studies of brain functional connectivity: the state of the art. Front Psychol. 2015; 6: 1–18. https://doi.org/10.3389/fpsyg.2015.00001 PMID: 25688217

66. Li HJ, Hou XH, Liu HH, Yue CL, Lu GM, Zuo XN. Putting age-related task activation into large-scale brain networks: A meta-analysis of 114 fMRI studies on healthy aging. Neurosci Biobehav Rev. 2015; 57: 156–174. https://doi.org/10.1016/j.neubiorev.2015.08.013 PMID: 26318367

67. Siman-Tov T, Bosak N, Sprecher E, Paz R, Eran A, Aharon-Peretz J, et al. Early age-related functional connectivity decline in high-order cognitive networks. Front Aging Neurosci. 2017; 8: 1–17. https://doi.org/10.3389/fnagi.2016.00330 PMID: 28119599

68. Davis SW, Dennis NA, Daselaar SM, Fleck MS, Cabeza R. Qué PASA? the posterior-anterior shift in aging. Cereb Cortex. 2008; 18: 1201–1209. https://doi.org/10.1093/cercor/bhm155 PMID: 17925295

69. Ezaki T, Fonseca dos Reis E, Watanabe T, Sakaki M, Masuda N. Closer to critical resting-state neural dynamics in individuals with higher fluid intelligence. Commun Biol. 2020; 3: 52. https://doi.org/10.1038/s42003-020-0774-y PMID: 32015402

70. Cole MW, Yarkoni T, Repovš G, Anticevic A, Braver TS. Global connectivity of prefrontal cortex predicts cognitive control and intelligence. J Neurosci. 2012; 32: 8988–8999. https://doi.org/10.1523/JNEUROSCI.0536-12.2012 PMID: 22745498

71. Beason-Held LL, Kraut MA, Resnick SM. Stability of default-mode network activity in the aging brain. Brain Imaging Behav. 2009; 3: 123–131. https://doi.org/10.1007/s11682-008-9054-z PMID: 19568331

72. Menon V, Uddin LQ. Saliency, switching, attention and control: a network model of insula function. Brain Struct Funct. 2010; 214: 655–667. https://doi.org/10.1007/s00429-010-0262-0 PMID: 20512370

73. Vossel S, Geng JJ, Fink GR. Dorsal and Ventral Attention Systems. Neurosci. 2014; 20: 150–159. https://doi.org/10.1177/1073858413494269 PMID: 23835449

74. Luo N, Sui J, Abrol A, Lin D, Chen J, Vergara VM, et al. Age-related structural and functional variations in 5,967 individuals across the adult lifespan. Hum Brain Mapp. 2020; 41: 1725–1737. https://doi.org/10.1002/hbm.24905 PMID: 31876339

75. Andrews-Hanna JR, Snyder AZ, Vincent JL, Lustig C, Head D, Raichle ME, et al. Disruption of Large-Scale Brain Systems in Advanced Aging. Neuron. 2007; 56: 924–935. https://doi.org/10.1016/j.neuron.2007.10.038 PMID: 18054866

76. Alam S, Kwon GR. Alzheimer disease classification using KPCA, LDA, and multi-kernel learning SVM. Int J Imaging Syst Technol. 2017; 27: 133–143. https://doi.org/10.1002/ima.22217

77. Xiong T, Cherkassky V. A combined SVM and LDA approach for classification. Proc Int Jt Conf Neural Networks. 2005; 3: 1455–1459. https://doi.org/10.1109/IJCNN.2005.1556089

78. Du Y, Fu Z, Calhoun VD. Classification and Prediction of Brain Disorders Using Functional Connectivity: Promising but Challenging. Front Neurosci. 2018;12. https://doi.org/10.3389/fnins.2018.00012 PMID: 29410610

79. Meszlényi RJ, Buza K, Vidnyánszky Z. Resting State fMRI Functional Connectivity-Based Classification Using a Convolutional Neural Network Architecture. Front Neuroinform. 2017; 11: 1–12. https://doi.org/10.3389/fninf.2017.00001 PMID: 28154532

80. Suk H II, Wee CY, Lee SW, Shen D. State-space model with deep learning for functional dynamics estimation in resting-state fMRI. Neuroimage. 2016; 129: 292–307. https://doi.org/10.1016/j.neuroimage.2016.01.005 PMID: 26774612

81. Nieuwenhuis M, van Haren NEM, Hulshoff Pol HE, Cahn W, Kahn RS, Schnack HG. Classification of schizophrenia patients and healthy controls from structural MRI scans in two large independent samples. Neuroimage. 2012; 61: 606–612. https://doi.org/10.1016/j.neuroimage.2012.03.079 PMID: 22507227

82. Lui S, Zhou XJ, Sweeney JA, Gong Q. Psychoradiology: The Frontier of Neuroimaging in Psychiatry. Radiology. 2016; 281: 357–372. https://doi.org/10.1148/radiol.2016152149 PMID: 27755933